JGR Solid Earth

RESEARCH ARTICLE
10.1029/2024JB029446

Stability of H_2O-Rich Fluid in the Deep Mantle Indicated by the MgO-SiO_2-H_2O Phase Relations at 23 GPa and 2,000 K

Hongzhan Fei[1,2]

[1]Key Laboratory of Geoscience Big Data and Deep Resource of Zhejiang Province, School of Earth Sciences, Zhejiang University, Hangzhou, China, [2]Bayerisches Geoinstitut, University of Bayreuth, Bayreuth, Germany

Abstract The Earth's mantle contains significant amounts of water in the form of hydroxyl in hydrous minerals, nominally anhydrous minerals, and hydrous silicate melts. H_2O fluid is thought to be present only in the shallow regions because it will always dissolve tens of weight percent of silicates by forming hydrous silicate melt in the deep mantle. Here I investigated the phase relations in the MgO-SiO_2-H_2O system by high-pressure experiments at a pressure of 23 GPa and a temperature of 2,000 K, corresponding to the conditions at the bottom of the mantle transition zone and the topmost lower mantle. The experimental results indicate that hydrous melt can contain more than 90 wt.% of H_2O, that is, it becomes H_2O-rich fluid when coexists only with stishovite. In contrast, silicate-rich hydrous melt is formed when the system is enriched with MgO component. Therefore, H_2O-rich fluid may be stabilized in locally SiO_2-enriched rocks even at the topmost lower mantle, acting as a water source for the deep lower mantle by slab subduction. The H_2O fluid also provide a possible cause for the occurrence of natural ice-VII originated from 660 km depth.

Plain Language Summary Although liquid H_2O is widely distributed on the Earth surface and shallow mantle, it is supposed to be absent in the deep mantle (>100 km depth) because it will dissolve several tens weight percent of silicates from minerals and form hydrous silicate melts. Here I investigated the compositions of hydrous silicate melt coexisting with mantle minerals under the topmost lower mantle conditions near 660-km depth. I found that when hydrous silicate melt coexists with stishovite, a high-pressure form of quartz in the subducted slabs at lower mantle depth, the composition of the hydrous silicate melt will be close to pure H_2O, that is, H_2O fluid only dissolves a very tiny amount of SiO_2 (<10 wt.%) even under the topmost lower mantle pressure and temperature conditions. Therefore, liquid H_2O may be stabilized in the Earth's deep interior, especially in the subducted crust, which is enriched with silica. The liquid H_2O could be a water source for the deep lower mantle by slab subduction.

Key Points:

- Water content in hydrous silicate melt strongly depends on the coexisting solid phases in the MgO-SiO_2-H_2O system
- H_2O-rich fluid could be stabilized when it coexists only with stishovite under lower mantle conditions
- H_2O-rich fluid may be stored in locally stishovite-enriched rocks and transported to the deep mantle by slab subduction

Correspondence to:
H. Fei,
feihongzhan@zju.edu.cn

Citation:
Fei, H. (2024). Stability of H_2O-rich fluid in the deep mantle indicated by the MgO-SiO_2-H_2O phase relations at 23 GPa and 2,000 K. *Journal of Geophysical Research: Solid Earth*, *129*, e2024JB029446. https://doi.org/10.1029/2024JB029446

Received 2 MAY 2024
Accepted 8 JUL 2024

Author Contribution:
Conceptualization: Hongzhan Fei
Data curation: Hongzhan Fei
Formal analysis: Hongzhan Fei
Funding acquisition: Hongzhan Fei
Investigation: Hongzhan Fei
Methodology: Hongzhan Fei
Project administration: Hongzhan Fei
Validation: Hongzhan Fei
Visualization: Hongzhan Fei
Writing – original draft: Hongzhan Fei
Writing – review & editing: Hongzhan Fei

1. Introduction

Water is circulated and dynamically equilibrated between the Earth's surface and deep interior by geological processes such as slab subduction and magma upwelling (Hirschmann, 2006; Karato et al., 2020; Ohtani, 2021). The fundamental issue about water transportation and circulation is how water is stored in the deep mantle. It is known that water in the mantle is primarily held as bonded hydroxyl in the crystal structures of hydrous (Ghosh & Schmidt, 2014; Ohtani et al., 2001; Pamato et al., 2015) and nominally anhydrous minerals (e.g., olivine, wadsleyite, and ringwoodite) (Bell & Rossman, 1992; Bolfan-Casanova, 2005; Druzhbin et al., 2021; Fei & Katsura, 2020, 2021; Kohlstedt et al., 1996) and as hydroxyl species in water-induced hydrous silicate melts (Fei, 2021; Ghosh & Schmidt, 2014; Hirth & Kohlstedt, 1996; Kushiro, 1972; Melekhova et al., 2007; Nakajima et al., 2019; O'Hara, 1965; Schmandt et al., 2014). In contrast, the pure or nearly pure H_2O fluid phase is thought to be present only in the shallow mantle (e.g., less than about 100 km depth) (Bureau & Keppler, 1999; Shen & Keppler, 1997; Wang et al., 2021). That is because at deep mantle temperatures (usually higher than ~1,500 K at more than ~100 km depth), H_2O fluid will always dissolve several tens weight percent of silicates from minerals and form silicate-rich hydrous melts (Fei, 2021; Ghosh & Schmidt, 2014; Myhill et al., 2017; Nakajima et al., 2019; Stalder et al., 2001) due to the miscibility of silicate melt and H_2O fluid (Bureau & Keppler, 1999).

Experimental investigations show that the water content in hydrous silicate melt depends on the pressure and temperature conditions (Drewitt et al., 2022; Fei, 2021; Ghosh & Schmidt, 2014; Nakajima et al., 2019). It decreases significantly from about 50 wt.% to 10 wt.% with increasing temperature from 1,600 to 2,300 K at 23–23.5 GPa, corresponding to the pressure conditions at the bottom of the mantle transition zone and the

topmost lower mantle near 660 km depth (Fei, 2021; Nakajima et al., 2019). The composition of the silicate melt will be close to H_2O fluid at 23–23.5 GPa only if the temperature is lower than ∼1,400 K when very tiny amounts of silicate can be dissolved in H_2O (Fei, 2021), that is, a temperature condition significantly lower than the mantle geotherm at 660 km depth (∼2,000 K, Katsura, 2022). On the other hand, since the solidus temperatures of peridotite increase with pressure (Takahashi, 1986; Zhang & Herzberg, 1994), the water content in hydrous melt within the peridotite–H_2O system is expected to increase with increasing pressure.

The decrease of water content in hydrous melt with temperature, however, is against the recently reported positive temperature dependence of water solubility in stishovite at 22–28 GPa, 1,300–2,270 K (Ishii et al., 2022; Purevjav et al., 2024). Since the melt fraction in the silicate mineral + hydrous melt system increases with increasing temperature, the water content in melt decreases (Fei, 2021), leading to a decrease in water activity in melt. As a result, the water content in the solid minerals should decrease, as confirmed experimentally in most mantle minerals (e.g., wadsleyite, ringwoodite, and majorite, Demouchy et al., 2005; Fei & Katsura, 2020, 2021; Litasov et al., 2011; Liu et al., 2024). In contrast, the positive temperature dependence of water solubility in stishovite (Ishii et al., 2022; Purevjav et al., 2024) (and in olivine at <1,520 K as well, Bali et al., 2008; Smyth et al., 2006; Zhao et al., 2004) suggests that the melt fraction does not increase significantly with temperature. Namely, the melt composition might be close to pure H_2O fluid in the stishovite + melt system.

Naturally formed ice-VII inclusions originated from the mantle transition zone or topmost lower mantle near the 660-km depth boundary were recently discovered within diamond (Tschauner et al., 2018). Since hydrous silicate melts contain ∼20 wt.% of H_2O and ∼80 wt.% silicates when coexisting mantle minerals (bridgmanite, ferropericlase, or ringwoodite) at 660-km depth temperatures of 2,000 K (Amulele et al., 2021; Drewitt et al., 2022; Fei, 2021; Ghosh & Schmidt, 2014; Nakajima et al., 2019), ice-VII and silicate mineral inclusions should be formed simultaneously during the solidification of hydrous melt. Therefore, although the ice-VII inclusions could be precipitated from hydrous melt, they might be also formed directly from H_2O fluid as well since they are isolated from other silicate inclusions.

The above factors suggest the possibility that a nearly pure H_2O phase, that is, a H_2O-rich fluid with a composition close to pure H_2O, might be stabilized under deep mantle conditions in a SiO_2-rich system. This is also supported by the variation of melt composition from SiO_2-rich to MgO-rich with increasing pressure (Ghosh & Schmidt, 2014; Kawamoto et al., 2004; Kawamoto et al., 2004, 2004; Komabayashi et al., 2004; Melekhova et al., 2007; Myhill et al., 2017; Novella et al., 2017; Stalder et al., 2001). Obviously, the phase relation and the water content in melt, in particular for the SiO_2-rich system, are the key for understanding the stability of H_2O-rich fluid in the deep mantle.

For a SiO_2-rich bulk composition, the water content in the melt of the SiO_2-H_2O endmember system was found to increase with pressure at <1 GPa (Kennedy et al., 1962). However, the phase relations and water contents in melts at higher pressures are poorly constrained. Here I investigated the phase relation in the silicate–H_2O system under both MgO-rich and SiO_2-rich conditions by high-pressure multi-anvil experiments at a pressure of 23 GPa and a temperature of 2,000 K, corresponding to the 660-km depth conditions. To uniquely constrain the phase rule, experiments were performed in a simplified system (MgO–SiO_2–H_2O ternary system).

2. Methods

2.1. Starting Materials

Mixtures with various bulk compositions (various Mg/Si molar ratios and various bulk H_2O contents as listed in Table 1) prepared from commercial MgO, SiO_2, and brucite powders, as well as SiO_2-gel beads, with purity of >99.9 wt.% were used as the starting materials. The MgO, SiO_2, and brucite have initial grain sizes of about 1 μm, while the SiO_2-gel beads have particle sizes of 3–5 mm and were grinded to powder with a ∼10-μm particle size. The MgO and SiO_2 powders were dried at 1,270 K, the brucite powder was dried at 400 K, and the SiO_2 gel powder was dried at 350 K prior to use. The water content in the 350-K dried SiO_2-gel was about 8.4 wt.% measured by mass loss after dehydration at 1,270 K. All powders were weighed following the desired bulk compositions with Mg/Si ratios and water contents controlled by the ratios of $Mg(OH)_2$, MgO, SiO_2, and SiO_2-gel (Table 1). They were well mixed by repeatedly grinding in an agate mortar and further dried at 350 K to remove the absorbed moisture during grinding.

Table 1
Compositions of the Starting Materials, Phase Assemblages of the Run Products, and Compositions of the Liquid Phases

	Starting material				Run product			
Run no.	Starting material	Bulk composition[a]	Bulk C_{H2O}	Mg/Si molar ratio	Phases	Liquid fraction	C_{H2O} in liquid	Mg/Si molar ratio in liquid
H4797	SiO_2, brucite	$Mg_2Si_{1.1}O_{4.2}$ + 24.6 wt.%H_2O	19.7 wt.%	2/1.1	L	100 (−) wt.%	19.7 (−) wt.%	1.75 (10)
H4795	SiO_2, brucite	$Mg_2Si_{1.1}O_{4.2}$ + 24.6 wt.%H_2O	19.7 wt.%	2/1.1	L	100 (−) wt.%	19.7 (−) wt.%	1.77 (14)
H4775[b]	MgO, SiO_2, brucite	Mg_2SiO_4 + 5 wt.%H_2O	4.76 wt.%	2/1	L + Rwd	20.3 (11) wt.%	21.4 (38) wt.%	2.35 (18)
H4805[b]	MgO, SiO_2, brucite	Mg_2SiO_4 + 15 wt.%H_2O	13.0 wt.%	2/1	L + Rwd	57.0 (38) wt.%	22.2 (18) wt.%	1.89 (5)
H5476	MgO, SiO_2, brucite	$MgSi_2O_5$ + 8.7 wt.%H_2O	8.0 wt.%	1/2	L + Sti + Aki	29.7 (6) wt.%	26.9 (5) wt.%	2.49 (9)
H5478	brucite, SiO_2-gel	$MgSi_5O_{11}$ + 13.4 wt.%H_2O	11.8 wt.%	1/5	L + Sti	25.9 (6) wt.%	45.5 (11) wt.%	2.92 (18)
S7794	brucite, gel	$MgSi_{10}O_{21}$ + 11.4 wt.%H_2O	10.2 wt.%	1/10	L + Sti	25.6 (80) wt.%	40.0 (90) wt.%	1.97 (72)
H5521A	SiO_2-gel	SiO_2 + 9.2 wt.%H_2O	8.40 wt.%	0/1	L + Sti	8.4 (5) wt.%	99.6 (55) wt.%	0.03 (5)
H5606A	brucite, SiO_2-gel	$MgSi_{30}O_{61}$ + 9.9 wt.%H_2O	9.05 wt.%	1/30	L + Sti	10.2 (1) wt.%	88.6 (80) wt.%	0.05 (10)
H5606B	brucite, SiO_2-gel	$MgSi_3O_7$ + 15.7 wt.%H_2O	13.5 wt.%	1/3	L + Sti	41.8 (16) wt.%	32.4 (12) wt.%	2.44 (15)
S7797A	MgO, SiO_2, brucite	$Mg_{20}SiO_{22}$ + 15 wt.%H_2O	13.0 wt.%	20/1	L + Per	33.9 (8) wt.%	38.4 (9) wt.%	4.07 (8)
S7797B	SiO_2, brucite	$Mg_{10}SiO_{11}$ + 38.9 wt.%H_2O	28.0 wt.%	10/1	L + Per	66.3 (45) wt.%	42.3 (27) wt.%	5.66 (48)
H5521B	MgO, brucite	MgO + 29.8 wt.%H_2O	23.0 wt.%	1/0	L + Per	43.9 (55) wt.%	52.2 (22) wt.%	181 (46)

Note. All experiments were performed at 23 GPa and 2,000 K with starting materials prepared from MgO, SiO_2, brucite, and SiO_2-gel. The uncertainties about the liquid fractions and C_{H2O} in the liquids are calculated based on the uncertainties in the EPMA analyses of the liquid phases. L, liquid phase; Rwd, ringwoodite (Mg_2SiO_4); Aki, akimotoite ($MgSiO_3$); Per, periclase (MgO); Sti, stishovite (SiO_2). [a]The bulk composition means 100 wt.% silicate plus 5–38.9 wt.% H_2O, for example, $Mg_2Si_{1.1}O_{4.2}$ + 24.6 wt.% H_2O means 100 wt.% $Mg_2Si_{1.1}O_{4.2}$ + 24.6 wt.% H_2O, therefore, the bulk H_2O content is 19.7 wt.%. [b]The runs H4775 and H4805 are already reported in Fei (2021). The Fe-bearing experiments in Fei (2021) are not discussed here because the FeO (and Fe_2O_3) component will introduce additional degrees of freedom in the phase rule. But the water content in Fe-bearing melt was within experimental uncertainty comparable to or only slightly lower than Fe-free melt (Fei, 2021).

2.2. High Pressure Experiments

By arc-welding, the mixtures were sealed in Pt-Rh capsules with outer and inner diameters of 1.2 and 1.0 mm, respectively. The lengths of the capsules were 1.0–1.2 mm. In each high-pressure run, one or two capsules were placed into a 10/4 multi-anvil cell assembly with a $LaCrO_3$ furnace and a ZrO_2 thermal insulator (standard 10/4 assembly at Bayerisches Geoinstitut). The assembly was compressed to a pressure of 23 GPa using a Kawai-type multi-anvil apparatus at room temperature, followed by heating at 2,000 K for a duration of 20–300 min, monitored by a D-type (W75%Re25%–W97%Re3%) thermocouple. After heating, the assembly was quenched to room temperature by shutting off the heating power and decompressed to ambient pressure over a duration of >15 hr.

By slightly puncturing the sample capsules after high pressure experiments, running fluid water was observed to escape from the capsules, indicating water-saturated conditions. Transparent crystals and white powders were observed within the capsules. In two runs (H5521A and H5606A), large caves with very tiny amounts of quenched crystals were found instead of white powder (Figure 1). Since running water was also observed in these two runs, the large caves were expected to be filled with H_2O. It should be emphasized that the absence of white powder is not caused by any material loss during cross-section preparation because the caves were observed

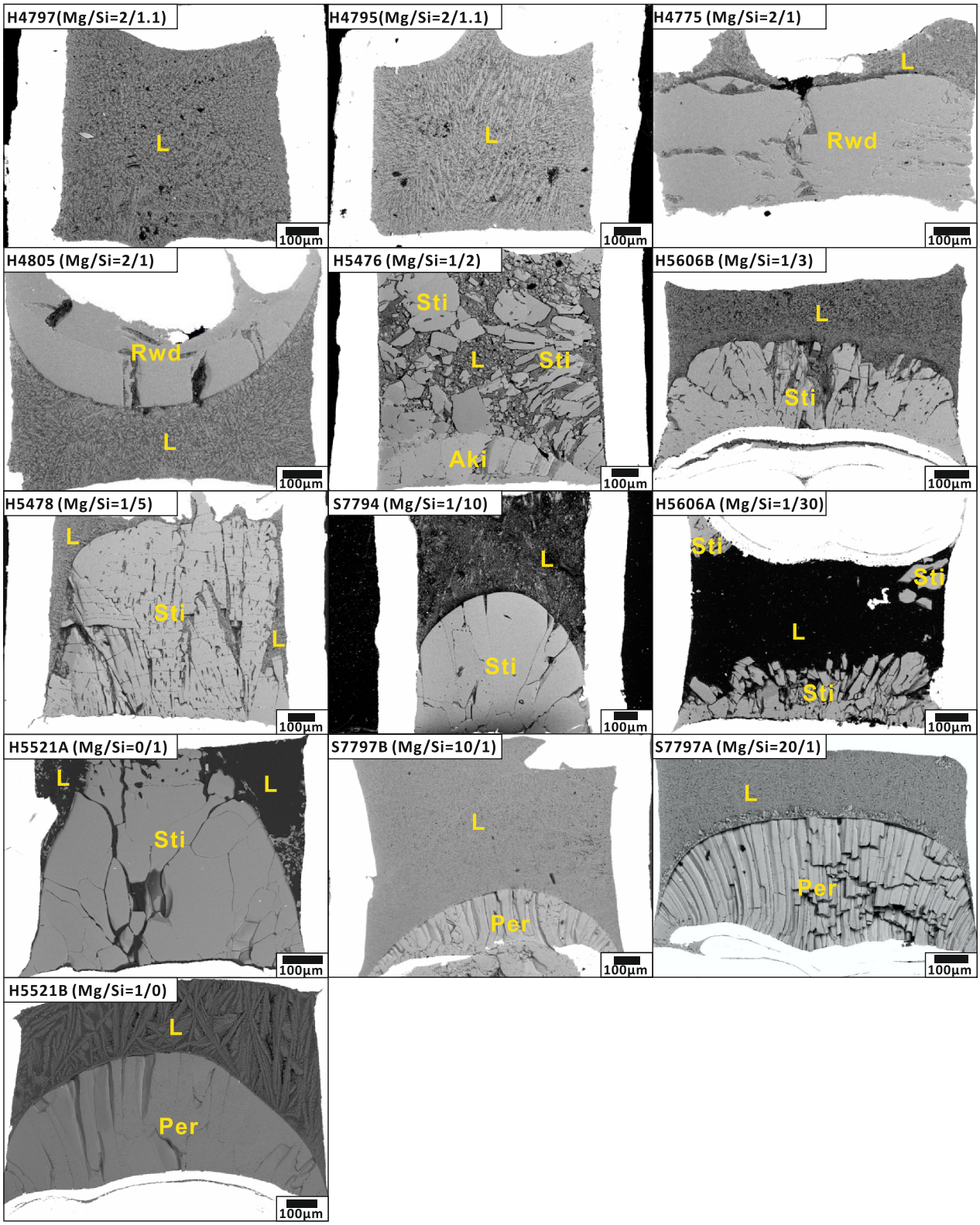

Figure 1. Backscattered electron images of all the recovered samples. The liquid phases appear as H_2O-rich fluid in H5521A and H5606A instead of quenched textures in other runs. A few crystals in H5606A were lost during polishing due to the poor sintering under water-saturated conditions. The capsule of S7797B is broken, which is caused by blow out during decompression. L, liquid phase (hydrous melt or H_2O-fluid); Sti, stishovite; Per, periclase; Aki, akimotoite.

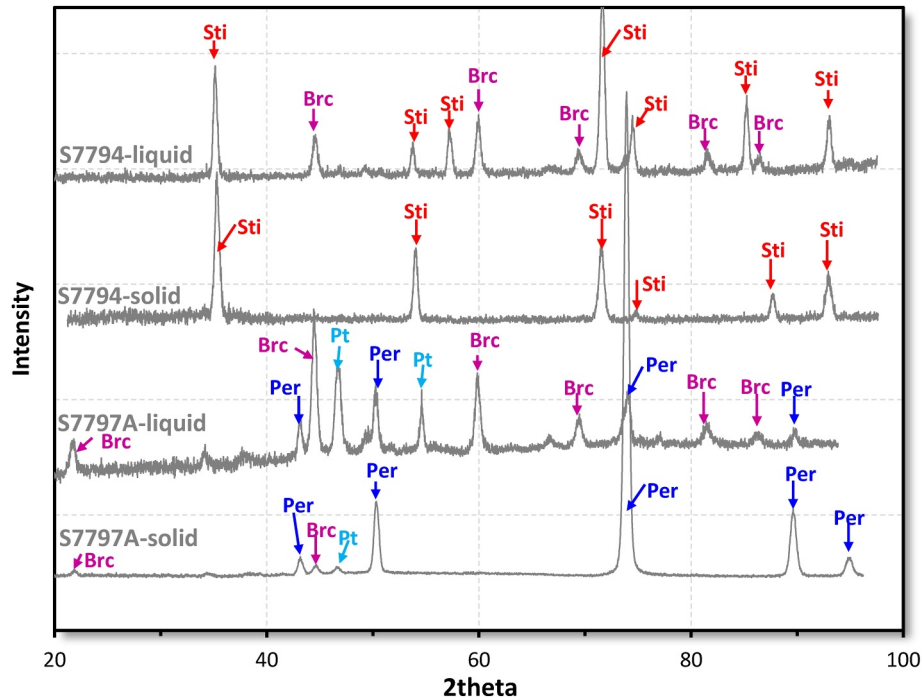

Figure 2. Examples of the X-ray diffraction spectra of the recovered samples. The stishovite, brucite, and periclase in the liquid phases should be formed by crystallization during quenching. Sti, stishovite; Brc, brucite; Per, periclase; Pt, platinum from the capsule.

during opening the capsule before polishing. Afterward, cross sections of capsules were prepared for the following analyses by mounting in epoxy and polishing with sandpaper and 1/4 μm diamond powder.

2.3. Sample Analyses

The phases in the run products were examined using a scanning electron microprobe (SEM) equipped with an energy-dispersive detector (EDS) (Zeiss LEO-1530) and a microfocus X-ray diffractometer (XRD) equipped with a Co source (Brucker AXS D8 Discover). The detailed analysis conditions for SEM and XRD are given elsewhere (Fei, 2021; Fei & Katsura, 2020, 2021). SEM images of all recovered samples are given in Figure 1, while examples of XRD spectra are shown in Figure 2.

The SiO_2 and MgO contents in the liquid phases were analyzed by a JEOL JXA-8200 electron probe microanalyzer (EPMA) with a wavelength-dispersive spectrometer (WDS). The acceleration voltage and current of the EPMA were 15 kV and 15 nA, respectively. A defocused beam with a 30–50 μm size was used. An enstatite crystal was used for the standard calibration. The EPMA results for the liquid phases are given in Table 1. The solid phases were examined by EPMA as well, using a focused beam. Since they are nearly pure periclase (MgO), akimotoite ($MgSiO_3$), ringwoodite ($Mg2SiO_4$), or stishovite (SiO_2), their compositions are not listed here, but the original data for both liquid and solid phases are given in Fei (2024).

2.4. Calculation of C_{H2O} in the Liquid Phases and the Experimental Uncertainty

Since crystallization of the silicate melt is inevitable during quenching in high-pressure experiments (Bondar et al., 2020), it is impossible to measure the water contents in the liquid phases directly in the recovered samples. Therefore, precise determination of the water contents of the liquid phases is challenging. A common method to estimate the water contents in crystallized liquid phases is mass balance calculation (Fei, 2021; Ghosh & Schmidt, 2014; Hirschmann et al., 2009; Novella et al., 2014), that is, the total amounts of SiO_2, MgO, and H_2O in the run products are equal to those in the starting materials. Thus, first, the mass fractions of the liquid phases were calculated from the MgO and SiO_2 contents in the starting materials (controlled by starting material preparation) and in the run products (obtained from EPMA analyses). Then, by assuming no water loss during experiments, the

water contents in the liquid phases were obtained from the bulk water contents in the starting material, fractions of the liquid phases in the run products, and water contents in the solid phases.

The water contents in the solid phases were taken from the water solubility experiments reported previously, that is, ∼1.0 wt.% in ringwoodite (Fei & Katsura, 2020), ∼0.04 wt.% in akimotoite (Bolfan-Casanova et al., 2000), <0.01 wt.% in periclase (Bolfan-Casanova et al., 2000), and <0.1 wt.% in Al-free stishovite (Liu et al., 2021; Purevjav et al., 2024) at 2,000 K. Note that, in comparison to the water contents in the liquid phase (several tens wt.% (Fei, 2021; Nakajima et al., 2019)), the solid phases have much lower water contents. Therefore, although the water solubilities in some minerals (e.g., bridgmanite) are still under debate (Fu et al., 2019; Liu et al., 2021), they have relatively small effects on the mass balance calculation. Additionally, it was reported that Al-free stishovite may have either very low water solubility (<0.1 wt.%) based on infrared analyses of single crystals recovered from multi-anvil high pressure experiments (Litasov et al., 2007; Liu et al., 2021; Purevjav et al., 2024) or very high water solubility (∼3.5 wt.% H_2O) based on the large unit cell volume compared to anhydrous stishovite in diamond anvil cell experiments (Lin et al., 2020, 2022; Nisr et al., 2020). The observed low water content was proposed to be caused by the ambient-pressure instability of high water-content stishovite (Li et al., 2023). However, recent in-situ multi-anvil experiments suggests that stishovite with large water-induced volume is metastable (Takaichi et al., 2024). Meanwhile, if stishovite in this study contains 3.5 wt.% of water (Lin et al., 2022), the silicate content in the liquid phase of H5606A would be ∼40 wt.%, which is against the observation of the absence of quenched crystals. Therefore, a water content of <0.1 wt.% in stishovite is more likely in this study.

As mentioned above, the calculation of water contents in the liquid phases requires the assumption of no water loss during experiments. Here I emphasize that, although protons in the form of H_2 may penetrate the metal capsules at high pressures easily, those in the form of hydroxyl or H_2O fluid can be well sealed (Eugster, 1957; Shaw, 1963). Especially, reduction of H_2O to H_2 is unlikely to occur in the Fe-free samples in this study. As detailed in the recent study (Fei, 2021), the water loss in high-pressure experiments is insignificant in case both ends of the capsules are well closed by arc-welding and the sample is free of or with relatively low contents of reducing components (such as organic carbon, metallic Fe, and FeO, all of which could reduce H_2O to H_2 easily). The insignificant water loss in this study is confirmed by the comparable melt fraction in experiments with different heating durations (from 5 to 1,800 min), by the systematic increase of melt fraction with increasing bulk water content in the starting materials, and by the consistent melt fractions and melt water contents obtained in different runs in Fei (2021). Therefore, the calculated water contents in the liquid phases by mass balance should be convincing despite the relatively large scattering of data points (Fei, 2021). Note that it is impractical to confirm the water loss or not by weighing the sample capsules before and after high pressure experiments because the sample volumes are extremely small. Meanwhile, the sample capsules were always stuck with tiny amounts of MgO from the high-pressure cell assemblies, denying the validity of measuring the capsule weight for the confirmation of water loss or not.

3. Results

3.1. Phase Assemblages in the Run Products

The transparent crystals (solid phases) are periclase (MgO) when the bulk Mg/Si molar ratio in the starting material is high, as demonstrated by X-ray diffraction (XRD) and SEM observations combined with energy dispersive spectroscopy (Figures 1 and 2, Table 1). By decreasing the Mg/Si ratio (adding the SiO_2 component), the solid phases appear to be one or two phases of ringwoodite (Mg_2SiO_4), akimotoite ($MgSiO_3$), and stishovite (SiO_2) sequentially. The grain sizes of the solid phases were tens to hundreds of microns (Figure 1). Fluid inclusions were observed in some of the stishovite crystals (Figure 1). Such inclusions should be trapped within the crystals during growth at high temperatures, but not due to the reduction of water solubility in stishovite during decompression (Lin et al., 2022), since diffusion of water in the crystals at room temperature should be limited and thus difficult to form large inclusions. The solid phases were absent in two runs (H4795 and H4797 in Table 1), which is reasonable because their bulk water contents were comparable to the water contents in hydrous melt (∼20 wt.%) under the experimental conditions (Fei, 2021), thus, complete melting had occurred. Large brucite crystals were absent in the capsules (only small crystals in the liquid phase regions with quenched texture formed by crystallization of melt during quenching, Figure 2), indicating the decomposition of brucite at high temperatures.

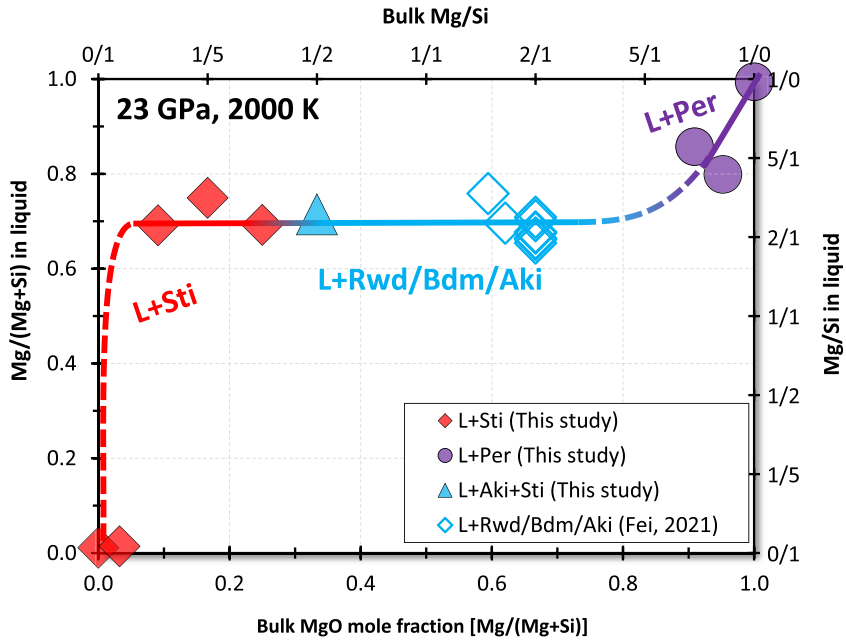

Figure 3. The composition of the liquid phase as a function of bulk composition of the starting material. The vertical axis is the molar fraction of MgO [calculated from Mg/(Mg + Si)] and Mg/Si molar ratio of the liquid phases in the recovered samples, while the horizontal axis is the bulk molar fraction of MgO and Mg/Si molar ratio in the starting materials. The Mg/Si molar ratios of the liquid phases are always larger than about 2.0 except those under extremely SiO_2-rich conditions. L, liquid phase; Sti, stishovite; Per, periclase; Rwd, ringwoodite; Bdm, bridgmanite; Aki, akimotoite.

3.2. Mg/Si Molar Ratios of the Liquid Phases

When complete melting has occurred, the compositions of the liquid phases are within analytical uncertainty identical to the starting materials (runs H4795 and H4797 with Mg/Si molar ratios of 1.75–1.77, Table 1). On the other hand, in the experiments performed in the SiO_2-H_2O (MgO-free) and MgO-H_2O (SiO_2-free) endmember systems, their liquid phases have extremely low and extremely high Mg/Si molar ratios, respectively (H5521A and H5521B, with Mg/Si molar ratios of 0.03 and 181, respectively, Figure 3, Table 1). Additionally, negligible amounts of silicates were detected in the liquid phase of H5606A (Table 1).

Except for the above runs, the Mg/Si molar ratios of the liquid phases are always ≥1.9 (Figure 3), which is more MgO-rich than the peridotitic composition (Mg/Si molar ratio ≈ 1.3). Even with extremely SiO_2-rich bulk compositions of starting materials (Mg/Si molar ratios of 1/5 and 1/10 in H5478 and S7794, respectively), the liquid phases are still enriched in MgO with Mg/Si molar ratio = 2–3 (Figure 3), leading to large amounts of stishovite crystals as the solid phase (Figure 1). These observations agree with the MgO-enrichment of hydrous melt reported previously (Amulele et al., 2021; Fei, 2021; Litasov & Ohtani, 2002; Nakajima et al., 2019).

3.3. Water Contents of the Liquid Phases

Because of the limited precision of mass balance calculations, the data points are relatively scattered, while the uncertainty of the data points primarily comes from the uncertainty of EPMA analyses (Table 1). Despite the experimental uncertainty, it is found that the water content of the liquid phase in the MgO-SiO_2-H_2O system strongly depends on the coexisting solid phases (Figure 4).

3.3.1. Coexistence of Liquid + Ringwoodite/Akimotoite/Bridgmanite

When the liquid phase coexists with ringwoodite or bridgmanite/akimotoite, it always contains 20–25 wt.% of water under pressure and temperature conditions of 23–23.5 GPa and 2,000 K, respectively (Figure 4 and Fei, 2021). In particular, with three coexisting phases (liquid + akimotoite + stishovite in H5476) in the MgO-SiO_2-H_2O ternary system, the water content in the liquid should be uniquely fixed by the phase rule. The water content value of about 20 wt.% is also confirmed by the occurrence of close to complete melting in experiments

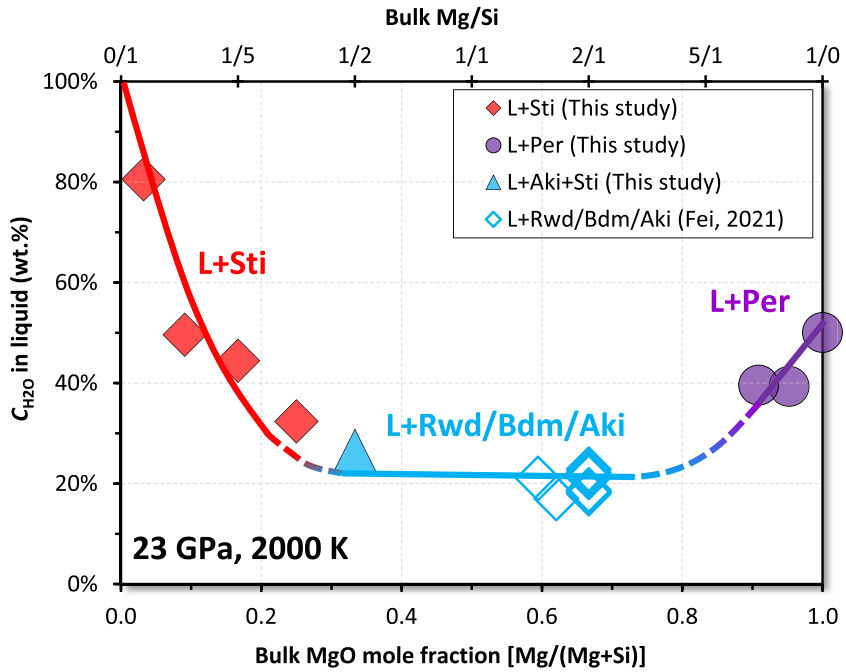

Figure 4. The water content of the liquid phase as a function of the bulk composition of the starting material. The horizontal axis represents the bulk mole fraction of MgO calculated from Mg/(Mg + Si) and the bulk Mg/Si molar ratio in the starting materials. The water content is found to be strongly dependent on the coexisting phases. It could reach ~90% (nearly pure H_2O fluid) when coexisting with only stishovite. L, liquid phase; Sti, stishovite; Per, periclase; Rwd, ringwoodite; Bdm, bridgmanite; Aki, akimotoite.

with bulk water contents of 18 wt.% (Fei, 2021) and complete melting in experiments with bulk water contents of 20 wt.% (H4795 and H4797 in this study).

A water content of about 20–40 wt.% in the liquid phase has been reported previously when coexisting with bridgmanite, akimotoite, davemaoite, and ferropericlase (Ghosh & Schmidt, 2014; Nakajima et al., 2019). Although they did not systematically investigate the temperature dependence of water content, their results generally agree with Fei (2021), which shows a temperature-dependent water content of ~10–50 wt.% at 1,600–2,300 K. In contrast, Amulele et al. (2021) reported a water content of 1–15 wt.% in liquid at 1,870 K and 25 GPa, a value comparable with the bulk water contents in their starting materials. This is unreasonable because the solids (primarily bridgmanite) have limited amounts of water, thus, the water in the system should be concentrated into liquid, leading to a much higher water content in the liquid phases than the bulk water contents in the starting materials.

3.3.2. Coexistence of Liquid + Periclase

With a high bulk MgO content in the system (Mg/Si molar ratio ≥10), the run products appear as coexistence of only liquid phase and periclase (Table 1). Since two phases coexist in the three-component system, the water content of the liquid phase is varied by the Mg/Si molar ratio of the starting material. With increasing Mg/Si ratio, the water content in liquid increases from 20–25 wt.% (the invariant point when coexisting with ringwoodite, akimotoite, or bridgmanite) to about 54 wt.% under SiO_2-free conditions (H5521B) (Figure 4).

3.3.3. Coexistence of Liquid + Stishovite

With high bulk SiO_2 content in the system (Mg/Si molar ratio ≤1/3), the run products show the liquid phase coexisting with only stishovite (Table 1). The water content in the liquid phase increases with increasing bulk SiO_2 content from 20 to 25 wt.% when coexisting with ringwoodite/akimotoite/bridgmanite in the MgO-SiO_2-H_2O ternary system to about 99 wt.% (nearly pure H_2O in run H5521A) in the SiO_2-H_2O binary system (Figure 4).

Table 2
Compositions of the Liquid Phases Obtained by EPMA Analyses

Run no.	*N*	MgO (wt.%)	SiO_2 (wt.%)	Total (wt.%)	Mg (atomic)	Si (atomic)
H4797	15	42.6 (20)	36.3 (8)	78.9 (21)	11.20 (33)	6.40 (17)
H4795	13	43.7 (18)	37.0 (21)	80.8 (23)	11.24 (47)	6.38 (24)
H4775[a]	9	43.3 (9)	27.6 (24)	70.9 (28)	12.96 (47)	5.52 (24)
H4805[a]	13	42.7 (9)	33.8 (0.8)	76.5 (14)	11.64 (17)	6.18 (9)
H5476	31	43.6 (12)	26.1 (9)	69.7 (17)	13.30 (23)	5.35 (11)
H5478	28	40.3 (10)	20.6 (10)	60.9 (11)	14.24 (35)	4.88 (17)
S7794	30	22.1 (53)	18.2 (59)	40.3 (85)	11.54 (210)	6.23 (105)
H5521A	31	0.1 (1)[b]	11.2 (50)	11.3 (50)	0.30 (56)	11.85 (28)
H5606A	23	0.02 (3)	0.7 (11)	0.7 (11)	0.52 (100)	11.74 (50)
H5606B	30	37.8 (14)	23.2 (18)	60.9 (30)	13.18 (36)	5.41 (18)
S7797A	18	48.5 (5)	17.8 (4)	66.2 (8)	16.09 (10)	3.96 (5)
S7797B	18	53.2 (14)	14.1 (9)	67.3 (10)	17.71 (39)	3.15 (19)
H5521B	25	47.8 (22)	0.4 (1)[b]	48.2 (21)	23.72 (7)	0.14 (3)

Note. *N* is the number of analyzed points. The error bar is one standard deviation from the *N* analyses. The atomic concentration is normalized to oxygen = 24. The totals are obtained by EPMA, which reflect the total mass of MgO and SiO_2 in EPMA analysis. [a]The compositions of H4775 and H4805 are from in Fei (2021). [b]The MgO component in H5521A and the SiO_2 component in H5521B are probably caused by contamination during sample polishing because their starting materials were respectively free of MgO and SiO_2.

It is noted that with high bulk SiO_2 content in the system (Mg/Si molar ratio ≤1/30 in H5521A and H5606A), the water contents in the liquid phase are 88–99 wt.% (Figure 4). Although this value may contain large uncertainty due to the uncertainties in EPMA analyses on the liquid phases and the limited precision of mass balance calculations, the following observations clearly demonstrate the stability of the H_2O-rich liquid phase in H5521A and H5606A: (a) The total weight percentage of the liquid phase from electron microprobe analysis is less than ~11 wt.% (Table 2). (b) Running water was observed when opening the sample capsules before polishing, leaving large caves instead of the crystallized melts observed in other runs. Specifically, the caves should be initially filled with water. (c) With increasing SiO_2 content in the starting material, the Mg/Si molar ratio of the liquid phase is always close to ~2.0 (Figure 3), namely, the composition of the liquid phase briefly follows the formula of $Mg_2SiO_4 \cdot nH_2O$. Therefore, the hydrous melt has an extremely high water-content when it coexists only with stishovite.

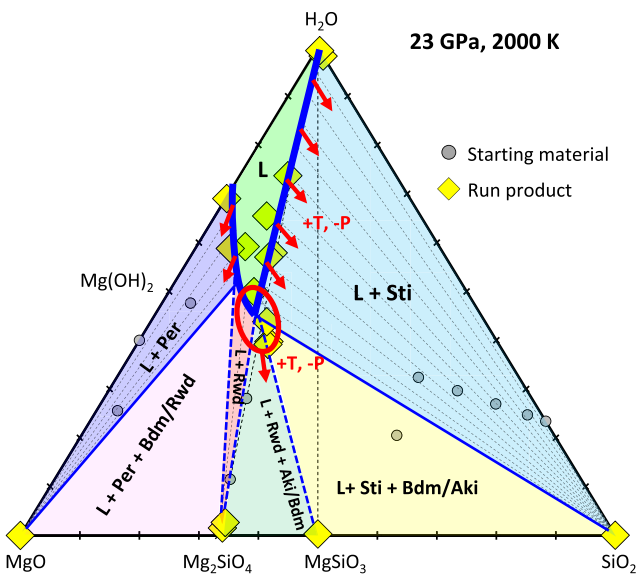

Figure 5. Phase relations of the SiO_2-MgO-H_2O ternary system at 23 GPa, 2,000 K in mole %. The water content in the liquid phase could reach >90 wt. % (H_2O-rich fluid) when the bulk composition is SiO_2-rich. The invariant point (marked by a red ellipse) is expected to move downward by either increasing the temperature or decreasing the pressure. L, liquid phase; Sti, stishovite; Per, periclase; Rwd, ringwoodite; Bdm, bridgmanite; Aki, akimotoite; P, pressure; T, temperature.

4. Discussions

4.1. Phase Relation of the MgO-SiO_2-H_2O System

Using the Mg/Si molar ratios and water contents in the liquid phases determined in this study, we can draw the phase diagram of the MgO-SiO_2-H_2O ternary system under the experimental pressure and temperature conditions (23 GPa, 2,000 K). As shown in Figure 5, when the bulk composition is MgO-enriched, the liquid phase coexists with periclase. It contains 20–54 wt.% water, depending on the bulk composition of the system. By increasing SiO_2 content in the system, ringwoodite, bridgmanite, or akimotoite appear, while the liquid phase contains 20%–25 wt.% water, uniquely constrained by the phase rule. Ringwoodite and akimotoite are stable at pressures below ~23 GPa and transfer to bridgmanite + periclase at higher pressures (Ishii et al., 2018). By further increasing SiO_2 content, periclase, ringwoodite, and

bridgmanite/akimotoite disappear sequentially because the MgO component is all taken by the liquid phase, as a result, only stishovite is stabilized as the solid phase (Figure 5). The coexisting liquid phase contains ∼20 to ∼99 wt.% of water, depending on the Mg/Si ratio in the system.

Based on the water contents in the liquid phases, it is expected that when the bulk Mg/Si molar ratio in the system is 2.0 (olivine composition), a bulk water content of about 20 wt.% is required for complete melting at 2,000 K. With an either higher or lower bulk Mg/Si molar ratio, a higher bulk water content is required. Complete melting will not occur in the SiO_2-H_2O binary system if the bulk water content is below 90 wt.%.

Of course, the phase relations in Figure 5 should be temperature- and pressure-dependent. At temperatures higher than 2,000 K, more silicate will be dissolved into the liquid phase, leading to a decrease of water content in the liquid phase (Fei, 2021; Ghosh & Schmidt, 2014; Melekhova et al., 2007). As a result, the stability field of the liquid phase will be expanded (the thick blue curve in Figure 5 moves downward with increasing temperature). In opposite, by decreasing temperature, the field of the liquid phase will shrink, while dense hydrous magnesium silicate (DHMS) phases will appear at temperatures below ∼1,600 K (Ghosh & Schmidt, 2014; Nishi et al., 2014; Ohtani et al., 2000, 2001). On the other hand, the Mg/Si molar ratio of the liquid phase (or (Mg + Fe)/Si ratio in a Fe-bearing system) may decrease slightly with increasing temperature (Fei, 2021; Ghosh & Schmidt, 2014; Melekhova et al., 2007). Meanwhile, because the solidus and liquidus temperatures of rocks increase with increasing pressure (Zhang & Herzberg, 1994), the silicate content in the liquid phase should decrease, resulting in the shrinking of the liquid phase stability field in Figure 5. Therefore, the water content in the liquid phase could be lower than 90 wt.% (hydrous silicate melt) if the experimental temperature is much higher or the pressure much lower than this study even in the endmember SiO_2-H_2O system.

The liquid phases in the stishovite–H_2O system were also investigated in Litasov et al. (2007), which showed a water content of 30–50 wt.% (based on their total mass of EPMA analysis) rather than a H_2O-rich fluid. However, it is not against the results in this study. That is because their experiments were performed either under lower pressure and higher temperature conditions than this study (20 GPa, 2,073 K) and thus more silicate can be dissolved into water, or with significant amounts of Al_2O_3 component (Al/Si molar ratio of 1/7–1/10, comparable to the Mg/Si molar ratio of 1/10 in run S7794 from this study).

4.2. Stability of H_2O-Rich Fluid in the Lower Mantle

Significant amounts of water could be transported to the deep mantle by subducted slabs (Hirschmann, 2006; Ohtani, 2020, 2021; Ohtani et al., 2018). The bulk slabs usually have a Mg/Si molar ratio of >0.2 (Gale et al., 2013), much higher than the SiO_2-rich experiments in this study (Mg/Si molar ratio ≤1/30). However, stishovite content may reach 25% in the basaltic layer and could be even higher (30%–40%) in the sedimentary layer of the subducted crusts at the mantle transition zone and topmost lower mantle depths (Irifune & Ringwood, 1987; Irifune et al., 1994; Ishii et al., 2022; Ono et al., 2001). Although other components such as MgO, FeO, Fe_2O_3, Al_2O_3, and CaO in the mantle may affect the phase relations of the SiO_2-H_2O system (upon the concentrations of those components, silicate-rich melt may be stabilized instead of H_2O-rich fluid), SiO_2 component could be concentrated locally in the SiO_2-rich rocks (e.g., quartz, agate, and opal aggregates in the crusts) and H_2O-rich fluid could be stabilized in such SiO_2-enriched regions. Therefore, in addition to the previously widely considered hydrous minerals, nominally anhydrous minerals, and silicate-rich hydrous melts (Bercovici & Karato, 2003; Hirschmann, 2006), water could be stored in the deep mantle in the form of H_2O-rich fluid as well.

The H_2O fluid phase may migrate upwards driven by buoyancy due to its smaller density than the solid phases (Sakamaki, 2017). It may dissolve the MgO component when encountering ultramafic mantle minerals (such as bridgmanite and ferropericlase) during upwelling, leading to the convection of H_2O-rich fluid into hydrous silicate melt. On the other hand, the subducted sediments may have lower density than the lower mantle materials near the 660-km boundary (Kawai et al., 2009, 2013), leading to the stagnation of the silica-rich sediments. The H_2O-rich fluid in the stagnated sediments may be trapped by diamond, providing a possible cause of the ice-VII inclusions originated from 660-km depth (Tschauner et al., 2018). Additionally, the H_2O fluid may be trapped in stishovite as inclusions (Figure 1), transported to the deep mantle by slab subduction and act as a water source for the lower mantle until the phase transition from stishovite to post-stishovite, which can dissolve significant amounts of water (1–3.5 wt.%, Ishii et al., 2022; Lin et al., 2022). Namely, all H_2O will be incorporated into the crystal structure of post-stishovite if the bulk water content is below the water solubility of post-stishovite.

5. Conclusions

In summary, high pressure multi anvil experiments at 23 GPa and 2,000 K on the phase relations of the MgO-SiO_2-H_2O system indicate that the water content of hydrous silicate melt is strongly correlated to the coexisting phases, which is controlled by the Mg/Si molar ratio in the system. When the system is enriched with SiO_2, hydrous silicate melt coexists with only stishovite, while its water content increases with increasing SiO_2 content in the system and may reach >90 wt.% in case the molar ratio of Mg/Si is smaller than 1/30. In contrast, the hydrous melt contains significant amounts of silicate when the bulk composition is mafic or ultramafic. Namely, a H_2O-rich fluid phase could be stabilized in the locally stishovite enriched regions at the mantle transition zone and topmost lower mantle depths.

Data Availability Statement

The EPMA and XRD data used in this paper are available at (Fei, 2024).

Acknowledgments

The author appreciates H. Fischer for high-pressure cell assembly preparation, Raphael Njul for sample polishing, Detlef Krauβe for EPMA calibration, and Narangoo Purevjav, Dan Liu for helpful discussion about water solubility in stishovite. Comments from Prof. Roland Stalder the anonymous reviewers, the editor, and associate editor are helpful for improving the manuscript. This work is financially supported by the Qizhen funding (Fundamental Research Funds for the Central Universities, No 2023QZJH06), the Startup Foundation for Hundred-Talent Program of Zhejiang University, and the annual budget of the Bayerisches Geoinstitut to H. Fei. Open Access funding enabled and organized by Projekt DEAL.

References

Amulele, G., Karato, S. I., & Girard, J. (2021). Melting of bridgmanite under hydrous shallow lower mantle conditions. *Journal of Geophysical Research: Solid Earth*, *126*(9), e2021JB022222. https://doi.org/10.1029/2021jb022222

Bali, E., Bolfan-Casanova, N., & Koga, K. T. (2008). Pressure and temperature dependence of H solubility in forsterite: An implication to water activity in the Earth interior. *Earth and Planetary Science Letters*, *268*(3–4), 354–363. https://doi.org/10.1016/j.epsl.2008.01.035

Bell, D. R., & Rossman, G. R. (1992). Water in Earth's mantle: The role of nominally anhydrous minerals. *Science*, *255*(5050), 1391–1397. https://doi.org/10.1126/science.255.5050.1391

Bercovici, D., & Karato, S. (2003). Whole-mantle convection and the transition-zone water filter. *Nature*, *425*(6953), 39–44. https://doi.org/10.1038/nature01918

Bolfan-Casanova, N. (2005). Water in the Earth's mantle. *Mineralien Magazine*, *69*(3), 229–257. https://doi.org/10.1180/0026461056930248

Bolfan-Casanova, N., Keppler, H., & Rubie, D. C. (2000). Water partitioning between normally anhydrous minerals in the MgO-SiO_2-H_2O system up to 24 GPa: Implications for the distribution of water in the Earth's mantle. *Earth and Planetary Science Letters*, *182*(3–4), 209–221. https://doi.org/10.1016/s0012-821x(00)00244-2

Bondar, D., Fei, H., Withers, A. C., & Katsura, T. (2020). A rapid-quench technique for multi-anvil high-pressure-temperature experiments. *Review of Scientific Instruments*, *91*(6), 065105. https://doi.org/10.1063/5.0005936

Bureau, H., & Keppler, H. (1999). Complete miscibility between silicate melts and hydrous fluids in the upper mantle: Experimental evidence and geochemical implications. *Earth and Planetary Science Letters*, *165*(2), 187–196. https://doi.org/10.1016/s0012-821x(98)00266-0

Demouchy, S., Deloule, E., Frost, D. J., & Keppler, K. (2005). Pressure and temperature-dependence of water solubility in Fe-free wadsleyite. *American Mineralogist*, *90*(7), 1084–1091. https://doi.org/10.2138/am.2005.1751

Drewitt, J. W. E., Walter, M. J., Brodholt, J. P., Muir, J. M. R., & Lord, O. T. (2022). Hydrous silicate melts and the deep mantle H_2O cycle. *Earth and Planetary Science Letters*, *581*, 117408. https://doi.org/10.1016/j.epsl.2022.117408

Druzhbin, D., Fei, H., & Katsura, T. (2021). Independent hydrogen incorporation in wadsleyite from oxygen fugacity and non-dissociation of H_2O in the reducing mantle transition zone. *Earth and Planetary Science Letters*, *557*, 116755. https://doi.org/10.1016/j.epsl.2021.116755

Eugster, H. P. (1957). Heterogeneous reactions involving oxidation and reduction at high pressures and temperatures. *Journal of Chemical Physics*, *26*(6), 1760–1761. https://doi.org/10.1063/1.1743626

Fei, H. (2021). Water content of the dehydration melting layer in the topmost lower mantle. *Geophysical Research Letters*, *48*(1), e2020GL090973. https://doi.org/10.1029/2020gl090973

Fei, H. (2024). Dataset for "Stability of H_2O-rich fluid in the deep mantle indicated by the MgO-SiO_2-H2O phase relations at 23 GPa and 2000 K" by H. Fei [Dataset]. *Zenodo*. https://doi.org/10.5281/zenodo.12616640

Fei, H., & Katsura, T. (2020). High water solubility of ringwoodite at mantle transition zone temperature. *Earth and Planetary Science Letters*, *531*, 115987. https://doi.org/10.1016/j.epsl.2019.115987

Fei, H., & Katsura, T. (2021). Water solubility in Fe-bearing wadsleyite at mantle transition zone temperatures. *Geophysical Research Letters*, *48*(9), e2021GL092836. https://doi.org/10.1029/2021gl092836

Fu, S., Yang, J., Karato, S. I., Vasiliev, A., Presniakov, M. Y., Gavriliuk, A. G., et al. (2019). Water concentration in single-crystal (Al, Fe)-bearing bridgmanite grown from the hydrous melt: Implications for dehydration melting at the topmost lower mantle. *Geophysical Research Letters*, *46*(17–18), 10346–10357. https://doi.org/10.1029/2019gl084630

Gale, A., Dalton, C. A., Langmuir, C. H., Su, Y., & Schilling, J. (2013). The mean composition of ocean ridge basalts. *Geochim. Geophys. Geosyst.*, *14*(3), 489–518. https://doi.org/10.1029/2012gc004334

Ghosh, S., & Schmidt, M. W. (2014). Melting of phase D in the lower mantle and implications for recycling and storage of H_2O in the deep mantle. *Geochimica et Cosmochimica Acta*, *145*, 72–88. https://doi.org/10.1016/j.gca.2014.06.025

Hirschmann, M. M. (2006). Water, melting, and the deep Earth H_2O cycle. *Annual Review of Earth and Planetary Sciences*, *34*(1), 629–653. https://doi.org/10.1146/annurev.earth.34.031405.125211

Hirschmann, M. M., Tenner, T., Aubaud, C., & Withers, A. C. (2009). Dehydration melting of nominally anhydrous mantle: The primacy of partitioning. *Physics of the Earth and Planetary Interiors*, *176*(1–2), 54–68. https://doi.org/10.1016/j.pepi.2009.04.001

Hirth, G., & Kohlstedt, D. L. (1996). Water in the oceanic upper mantle: Implications for rheology, melt extraction, and the evolution of the lithosphere. *Earth and Planetary Science Letters*, *144*(1–2), 93–108. https://doi.org/10.1016/0012-821x(96)00154-9

Irifune, T., & Ringwood, A. E. (1987). Phase transformations in primitive MORB and pyrolite compositions to 25 GPa and some geophysical implications. In M. Manghnani & Y. Syono (Eds.), *High pressure Research in mineral physics* (Eds., pp. 231–242).

Irifune, T., Ringwood, A. E., & Hibberson, W. O. (1994). Subduction of continental crust and terrigenous and pelagic sediments: An experimental study. *Earth and Planetary Science Letters*, *126*(4), 351–368. https://doi.org/10.1016/0012-821x(94)90117-1

Ishii, T., Criniti, G., Ohtani, E., Purevjav, N., Fei, H., Katsura, T., & Mao, H. K. (2022). Superhydrous aluminous silica phases as major water hosts in high-temperature lower mantle. *PNAS*, *119*(44), e2211243119. https://doi.org/10.1073/pnas.2211243119

Ishii, T., Huang, R., Fei, H., Koemets, I., Liu, Z., Maeda, F., et al. (2018). Complete agreement of the post-spinel transition with 660-km seismic discontinuity. *Scientific Reports*, *8*(1), 6358. https://doi.org/10.1038/s41598-018-24832-y

Karato, S. I., Karki, B., & Park, J. (2020). Deep mantle melting, global water circulation and its implications for the stability of the ocean mass. *Progress in Earth and Planetary Science*, *7*(1), 76. https://doi.org/10.1186/s40645-020-00379-3

Katsura, T. (2022). A revised adiabatic temperature profile for the mantle. *Journal of Geophysical Research: Solid Earth*, *127*(2), e2021JB023562. https://doi.org/10.1029/2021jb023562

Kawai, K., Tsuchiya, T., Tsuchiya, J., & Maruyama, S. (2009). Lost primordial continents. *Gondwana Research*, *16*(3–4), 581–586. https://doi.org/10.1016/j.gr.2009.05.012

Kawai, K., Yamamoto, S., Tsuchiya, T., & Maruyama, S. (2013). The second continent: Existence of granitic continental materials around the bottom of the mantle transition zone. *Geoscience Frontiers*, *4*, 1–6. https://doi.org/10.1016/j.gsf.2012.08.003

Kawamoto, T., Matsukage, K. N., Mibe, K., Isshiki, M., Nishimura, K., Ishimatsu, N., & Ono, S. (2004). Mg/Si ratios of aqueous fluids coexisting with forsterite and enstatite based on the phase relations in the Mg_2SiO_4-SiO_2-H_2O system. *American Mineralogist*, *89*(10), 1433–1437. https://doi.org/10.2138/am-2004-1010

Kennedy, G. C., Wasserburg, G. J., Heard, H. C., & Newton, R. C. (1962). The upper three-phase region in the system SiO_2-H_2O. *American Journal of Science*, *260*(7), 501–521. https://doi.org/10.2475/ajs.260.7.501

Kohlstedt, D. L., Keppler, H., & Rubie, D. C. (1996). Solubility of water in the α, β and γ phases of $(Mg, Fe)_2SiO_4$. *Contributions to Mineralogy and Petrology*, *123*(4), 345–357. https://doi.org/10.1007/s004100050161

Komabayashi, T., Omori, S., & Maruyama, S. (2004). Petrogenetic grid in the system MgO-SiO_2-H_2O up to 30 GPa, 1600°C: Applications to hydrous peridotite subducting into the Earth's deeper interior. *Journal of Geophysical Research: Solid Earth*, *109*(B3), B03206. https://doi.org/10.1029/2003jb002651

Kushiro, I. (1972). Effect of water on the composition of magmas formed at high pressures. *Journal of Petrology*, *13*(2), 311–334. https://doi.org/10.1093/petrology/13.2.311

Li, J., Lin, Y., Meier, T., Liu, Z., Yang, W., Mao, H. K., et al. (2023). Silica-water superstructure and one-dimensional superionic conduit in Earth's mantle. *Science Advances*, *9*(35), eadh3784. https://doi.org/10.1126/sciadv.adh3784

Lin, Y., Hu, Q., Meng, Y., Walter, M., & Mao, H. K. (2020). Evidence for the stability of ultrahydrous stishovite in Earth's lower mantle. *PNAS*, *117*(1), 184–189. https://doi.org/10.1073/pnas.1914295117

Lin, Y., Hu, Q., Walter, M., Yang, J., Meng, Y., Feng, X., et al. (2022). Hydrous SiO_2 in subducted oceanic crust and H_2O transport to the core-mantle boundary. *Earth and Planetary Science Letters*, *594*, 117708. https://doi.org/10.1016/j.epsl.2022.117708

Litasov, K., & Ohtani, E. (2002). Phase relations and melt compositions in CMAS-pyrolite-H_2O system up to 25 GPa. *Physics of the Earth and Planetary Interiors*, *134*(1–2), 105–127. https://doi.org/10.1016/s0031-9201(02)00152-8

Litasov, K. D., Kagi, H., Shatskiy, A., Ohtani, E., Lakshtanov, D. L., Bass, J. D., & Ito, E. (2007). High hydrogen solubility in Al-rich stishovite and water transport in the lower mantle. *Earth and Planetary Science Letters*, *262*(3–4), 620–634. https://doi.org/10.1016/j.epsl.2007.08.015

Litasov, K. D., Shatskiy, A., Ohtani, E., & Katsura, T. (2011). Systematic study of hydrogen incorporation into Fe-free wadsleyite. *Physics and Chemistry of Minerals*, *38*(1), 75–84. https://doi.org/10.1007/s00269-010-0382-3

Liu, D., Purevjav, N., Fei, H., Withers, A. C., Ye, Y., & Katsura, T. (2024). Temperature and compositional dependences of H_2O solubility in majorite. *American Mineralogist*. https://doi.org/10.2138/am-2023-9130

Liu, Z., Fei, H., Chen, L., McCammon, C., Wang, L., Liu, R., et al. (2021). Bridgmanite is nearly dry at the top of the lower mantle. *Earth and Planetary Science Letters*, *570*, 117088. https://doi.org/10.1016/j.epsl.2021.117088

Melekhova, E., Schmidt, M. W., Ulmer, P., & Pettke, T. (2007). The composition of liquids coexisting with dense hydrous magnesium silicates at 11–13.5GPa and the endpoints of the solidi in the MgO–SiO_2–H_2O system. *Geochimica et Cosmochimica Acta*, *71*(13), 3348–3360. https://doi.org/10.1016/j.gca.2007.03.034

Myhill, R., Frost, D. J., & Novella, D. (2017). Hydrous melting and partitioning in and above the mantle transition zone: Insights from water-rich MgO–SiO_2–H_2O experiments. *Geochimica et Cosmochimica Acta*, *200*, 408–421. https://doi.org/10.1016/j.gca.2016.05.027

Nakajima, A., Sakamaki, T., Kawazoe, T., & Suzuki, A. (2019). Hydrous magnesium-rich magma genesis at the top of the lower mantle. *Scientific Reports*, *9*(1), 7420. https://doi.org/10.1038/s41598-019-43949-2

Nishi, M., Irifune, T., Tsuchiya, J., Tange, Y., Nishihara, Y., Fujino, K., & Higo, Y. (2014). Stability of hydrous silicate at high pressures and water transport to the deep lower mantle. *Nature Geoscience*, *7*(3), 224–227. https://doi.org/10.1038/ngeo2074

Nisr, C., Chen, H., Leinenweber, K., Chizmeshya, A., Prakapenka, V. B., Prescher, C., et al. (2020). Large H_2O solubility in dense silica and its implications for the interiors of water-rich planets. *PNAS*, *117*(18), 9747–9754. https://doi.org/10.1073/pnas.1917448117

Novella, D., Dolejs, D., Myhill, R., Pamato, M. G., Manthilake, G., & Frost, D. J. (2017). Melting phase relations in the system Mg_2SiO_4-H_2O and $MgSiO_3$-H_2O and the formation of hydrous melts in the upper mantle. *Geochimica et Cosmochimica Acta*, *204*, 68–82. https://doi.org/10.1016/j.gca.2016.12.042

Novella, D., Frost, D. J., Hauri, E. H., Bureau, H., Raepsaet, C., & Roberge, M. (2014). The distribution of H_2O between silicate melt and nominally anhydrous peridotite and the onset of hydrous melting in the deep upper mantle. *Earth and Planetary Science Letters*, *400*, 1–13. https://doi.org/10.1016/j.epsl.2014.05.006

O'Hara, M. J. (1965). Primary magmas and the origin of basalts. *Scottish Journal of Geology*, *1*, 19–40. https://doi.org/10.1144/sjg01010019

Ohtani, E. (2020). The role of water in Earth's mantle. *National Science Review*, *7*(1), 224–232. https://doi.org/10.1093/nsr/nwz071

Ohtani, E. (2021). Hydration and dehydration in Earth's interior. *Annual Review of Earth and Planetary Sciences*, *49*(1), 253–278. https://doi.org/10.1146/annurev-earth-080320-062509

Ohtani, E., Mizobata, H., & Yurimoto, H. (2000). Stability of dense hydrous magnesium silicate phases in the systems Mg_2SiO_4-H_2O and $MgSiO_3$-H_2O at pressures up to 27 GPa. *Physics and Chemistry of Minerals*, *27*(8), 533–544. https://doi.org/10.1007/s002690000097

Ohtani, E., Toma, M., Litasov, K., Kubo, T., & Suzuki, A. (2001). Stability of dense hydrous magnesium silicate phases and water storage capacity in the transition zone and lower mantle. *Physics of the Earth and Planetary Interiors*, *124*(1–2), 105–117. https://doi.org/10.1016/s0031-9201(01)00192-3

Ohtani, E., Yuan, L., Ohira, I., Shatskiy, A., & Litasov, K. (2018). Fate of water transported into the deep mantle by slab subduction. *Journal of Asian Earth Sciences*, *167*, 2–10. https://doi.org/10.1016/j.jseaes.2018.04.024

Ono, S., Ito, E., & Katsura, T. (2001). Mineralogy of subducted basaltic crust (MORB) from 25 to 37 GPa and chemical heterogeneity of the lower mantle. *Earth and Planetary Science Letters*, *190*(1–2), 57–63. https://doi.org/10.1016/s0012-821x(01)00375-2

Pamato, M. G., Myhill, R., Boffa-Ballaran, T., Frost, D. J., Heidelbach, F., & Miyajima, N. (2015). Lower-mantle water reservoir implied by the extreme stability of a hydrous aluminosilicate. *Nature Geoscience*, *8*(1), 75–79. https://doi.org/10.1038/ngeo2306

Purevjav, N., Fei, H., Ishii, T., Criniti, G., Lin, Y., Mao, H. K., & Katsura, T. (2024). Temperature dependence of H_2O solubility in Al-free stishovite. *Geophysical Research Letters*, *51*(3), e2023GL104029. https://doi.org/10.1029/2023gl104029

Sakamaki, T. (2017). Density of hydrous magma. *Chemical Geology*, *475*, 135–139. https://doi.org/10.1016/j.chemgeo.2017.11.012

Schmandt, B., Jacobsen, S. D., Becker, T. W., Liu, Z., & Dueker, K. G. (2014). Dehydration melting at the top of the lower mantle. *Science*, *344*(6189), 1265–1268. https://doi.org/10.1126/science.1253358

Shaw, H. R. (1963). Hydrogen-water vapor mixtures: Control of hydrothermal atmospheres by hydrogen osmosis. *Science*, *139*(3560), 1220–1222. https://doi.org/10.1126/science.139.3560.1220

Shen, A. H., & Keppler, H. (1997). Direct observation of complete miscibility in the albite-H_2O system. *Nature*, *385*(6618), 710–712. https://doi.org/10.1038/385710a0

Smyth, J. R., Frost, D. J., Nestola, F., Holl, C. M., & Bromiley, G. (2006). Olivine hydration in the deep upper mantle: Effects of temperature and silica activity. *Geophysical Research Letters*, *33*(15), L15301. https://doi.org/10.1029/2006GL026194

Stalder, R., Ulmer, P., Thompson, A. B., & Günther, D. (2001). High pressure fluids in the system MgO-SiO_2-H_2O under upper mantle conditions. *Contributions to Mineralogy and Petrology*, *140*(5), 607–618. https://doi.org/10.1007/s004100000212

Takahashi, E. (1986). Melting of a dry peridotite KLB-1 up to 14 GPa: Implications on the origin of peridotitic upper mantle. *Journal of Geophysical Research*, *91*(B9), 9367–9382. https://doi.org/10.1029/jb091ib09p09367

Takaichi, G., Nishihara, Y., Matsukage, K. N., Nishi, M., Higo, Y., Tange, Y., et al. (2024). Limited stability of hydrous SiO_2 stishovite in the deep mantle. *Earth and Planetary Science Letters*, *640*, 118790. https://doi.org/10.1016/j.epsl.2024.118790

Tschauner, O., Huang, S., Greenberg, E., Prakapenka, V. B., Ma, C., Rossman, G. R., et al. (2018). Ice-VII inclusions in diamonds: Evidence for aqueous fluid in Earth's deep mantle. *Science*, *359*(6380), 1136–1139. https://doi.org/10.1126/science.aao3030

Wang, Q. X., Zhou, D. Y., Li, W. C., & Ni, H. W. (2021). Spinodal decomposition of supercritical fluid forms melt network in a silicate-H_2O system. *Geochem. Persp. Lett.*, *18*, 22–26. https://doi.org/10.7185/geochemlet.2119

Zhang, J., & Herzberg, C. (1994). Melting experiments on anhydrous peridotite KLB-1 from 5.0 to 22.5 GPa. *Journal of Geophysical Research: Solid Earth*, *99*(B9), 17729–17742. https://doi.org/10.1029/94jb01406

Zhao, Y., Ginsberg, S. B., & Kohlstedt, D. L. (2004). Solubility of hydrogen in olivine: Dependence on temperature and iron content. *Contributions to Mineralogy and Petrology*, *147*(2), 155–161. https://doi.org/10.1007/s00410-003-0524-4